Microcapsule based self-healing for 3D printed polymer composites

by

Shreyas Devdutt Shelke

A thesis submitted to the Graduate Faculty of
Auburn University
in partial fulfillment of the
requirements for the Degree of
Master of Science, Polymer and Fiber Engineering

Auburn, Alabama
August 3rd, 2019

Keywords: Self-healing, Microcapsules, Additive manufacturing, polymer composites.

Approved by

Dr. Asha-Dee Celestine, Assistant Professor, Aerospace Engineering
Dr. Bryan Beckingham, Assistant Professor, Chemical Engineering
Dr. Maria Auad, Professor, Chemical Engineering

Abstract

Polymer composites are widely used in many industries due to their superior properties. Many of these composites are 3D printed to allow for greater customization and control over the properties. However, the replacement of damaged/ faulty composites is very costly and time consuming. Therefore, there is a need for self-healing composites which can recover its properties even after a damage event. Self-healing materials have gained increased traction among the research community, over the years, because of their inherent ability to detect and autonomously heal any damage to the material system. Various attempts have been made to develop increasingly efficient self-healing systems and their eventual integration in polymers at a large scale. There are three main approaches for achieving self-healing properties in a material system: microcapsule-based healing systems, vascular-based healing systems, and intrinsic healing systems. This research is focused on the preparation of a self-healing system with microcapsules as their healing agents. High impact polystyrene (HIPS) and Polylactic acid (PLA), which are two materials that exhibit excellent 3D printing properties are to be used as the bulk polymer in these systems. The polymer samples were made using a combination of solvent casting and melt casting techniques. Comparative tests of samples with and without the self-healing microcapsules were conducted to determine the effect of the microcapsules on the virgin and self-healing properties of HIPS and PLA. Characterization included differential scanning calorimetry, thermogravimetric analysis, optical microscopy, scanning electron microscopy, dynamic mechanical analysis, flexure as well as fracture tests to evaluate healing efficiency.

Acknowledgments

Throughout the writing of this thesis, I have received a great deal of support and assistance. I would first like to thank my supervisor, Dr. Asha-Dee Celestine, whose expertise was invaluable in the formulating of the research topic and methodology in particular. I would particularly like to single out my Head of Department, Dr. Maria Auad. Dr. Auad, I want to thank you for the opportunity I was given to conduct my research and further my dissertation with Dr. Celestine. I would also like to thank Dr. Bryan Beckingham, for his valuable guidance throughout this project. You provided me with the tools and the lab that I needed to successfully complete my dissertation. Special thanks to Dr. Uday Vaidya and Dr. Nitilaksh Hiremat at the University of Tennessee-Knoxville for performing DMA experiments. In addition, I would like to thank my parents and my significant other, for their wise counsel and sympathetic ear. You are always there for me. Finally, there are my friends, who were of great support in deliberating over our problems and findings, as well as providing a happy distraction to rest my mind outside of my research.

Table of Contents

List of Illustrations

List of Abbreviations

AM Additive Manufacturing

HIPS High Impact Polystyrene

PU Polyurethane

THF Tetrahydrofuran

DSC Differential Scanning Calorimeter

EPA Ethyl Phenylacetate

PLA Polylactic Acid

1. Introduction

1.1 Self-healing

Self-healing can be defined as the ability of a material to repair any damage and restore lost properties, using resources inherently available to the material system [1-4]. These self-healing systems are inspired by the damage response of biological systems, which heal themselves without outside intervention, e.g. barks of trees that are damaged. Self-healing materials with a lot of inherently different properties are available depending on the end application [5]. Self-healing materials can be divided into two categories based on their damage response, autonomous and non-autonomous self-healing. Autonomous self-healing systems do not require any additional stimulus for the self-healing process to be initiated, because the material damage is enough to trigger the process [6-8]. Non-autonomous self-healing systems require an external stimulus to trigger and execute the self-healing process, e.g., light or heat. A human can initiate this stimulus, or it can be instigated by something that is already present in the working environment of the system [4].

Autonomous self-healing systems can be further divided into two categories depending on the type of healing mechanism employed. The first category is intrinsic self-healing materials. Intrinsic self-healing materials can heal themselves due to their inherent chemical structure, which may consist of various types of reversible bonds and reactions, such as hydrogen bonds or reversible covalent bonds formed by Diels-Alder cycloaddition e.g. using DCPD/ Grubb's catalyst [9-11]. Intrinsic self-healing materials possess a latent self-healing functionality that is usually triggered by damage or by an external stimulus such as heat and light. Conductive hydrogels that are capable of self-healing thanks to their base chemistry are a great example of intrinsic self-healing materials [12-13].

The second category of autonomous self-healing is extrinsic self-healing materials. In extrinsic systems, the healing agents are isolated in a separate phase from the host material using either microcapsules or vascular network systems. When the material is damaged, the microcapsules or vascular network rupture and release their self-healing contents into the crack plane, where it further reacts with the material initiating the process of self-healing [4]. Extrinsic self-healing systems are capable of achieving very high healing efficiencies, with over 100% healing possible, even when the damage is extensive [14]. One of the disadvantages of extrinsic self-healing as compared to intrinsic self-healing is that they offer a limited amount of healing. For example, once the microcapsules are empty, the material cannot be healed in that location later [4]. But, intrinsic self-healing needs chain mobility along the cracks to bring about self-healing and is viable mostly in non-tough materials like aerogels and elastomers, whereas extrinsic self-healing systems work well enough for all kinds of materials.

Extrinsic self-healing systems are further classified based on the method in which the self-healing material is contained. Microcapsule-based self-healing systems isolate the healing agents in micron-sized capsules and release the agents on being ruptured during a damage event. Microcapsule based self-healing systems can be achieved by four main sequestering methods. Capsule-catalyst system includes a system in which the catalyst is dispersed in the polymer bulk and the healing agent is encapsulated in the microcapsules [4]. The DCPD-Grubbs system is a great example of this system [10-11]. This self-healing system has already been successfully demonstrated in thermoset polymers by White et. al. [1, 15-16]. Another system is multi-capsule system in which all the required components for the self-healing process are sequestered in multiple microcapsule types. Phase separated microcapsule systems consists of at least one component that exists as a separate phase within the bulk polymer in addition to the microcapsules.

Finally, latent functionality is a type of microcapsule-based system and it makes use of the properties of bulk polymers, which react with the healing agents sequestered in the microcapsules for self-healing [17].

Solvent based self-healing which is a variant of latent functionality system is a useful system [18]. In solvent based self-healing systems, the self-healing fluid uses latent functionality of the bulk polymer to bring forth self-healing [18-19]. The working principle of this system is that when the microcapsules are ruptured, the solvent is released into the crack. This solvent locally dissolves the polymer and on evaporating leaves behind a healed crack [4] [20-23]. Autonomous self-healing in PMMA was achieved by microencapsulated solvent by Celestine et al. which did not require a catalyst [24]. The main advantage of microcapsule system is that it is highly localized and can heal damage right where the crack is propagating. Its main disadvantage is that it can be used only once.

In a vascular self-healing system, the healing agent is sequestered in a network of capillary-sized hollow channels that can be interconnected in the material one-dimensionally, two-dimensionally, or three-dimensionally [25]. One advantage of this system is that once these hollow systems are damaged, the vascular system as a whole can be refilled with the healing fluid using an outside source or a vascular channel that is undamaged. It also has high self-healing efficiency because compared to the microcapsule based self-healing system, the healing fluid in the microvascular system has a higher probability of the healing agent coming in contact with the damage/crack due to the vascular system being evenly distributed throughout the bulk polymer. Thus, this leads to a higher healing agent volume to crack ratio and coupled with the reusability of vascular system is a good self-healing system for solvent-based self-healing. The disadvantage of a vascular system is that not all polymer structures allow for hollow channels as they can

compromise the mechanical properties [26-27]. Another limitation is the requirement of stacking the vascular networks in order to build the 3D structure. Figure 1.1 shows an example of both microcapsule as well as vascular based self-healing systems.

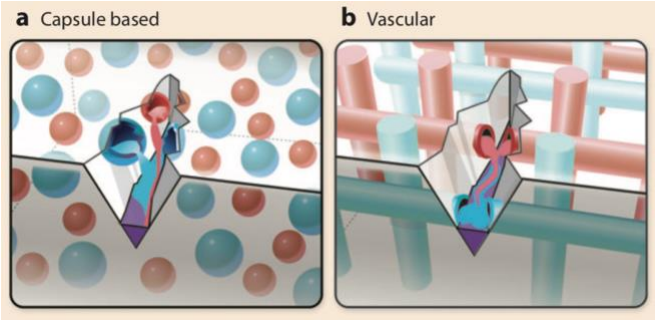

Figure 1.1 Schematic of self-healing mechanisms (a) capsule based (b) vascular based Image courtesy: B.J. Blaiszik (2010)

1.2 Additive manufacturing

Additive manufacturing (AM) is one of the optimal methods to manufacture self-healing materials due to the wide range of techniques available. Additive manufacturing (AM) are methods of fabrication that produce objects by various methods, one of which includes using extrusion for layer by layer addition of material [34]. Over the years, 3D printing technologies have gained rapid advancements. These methods have reached a state of all-time high popularity with the common masses and are becoming common knowledge even amongst people not from scientific fields [28-33]. AM is significantly different from conventional subtractive methods such as lathe machining and other traditional methods, which consist of chipping off the material until the desired shape is obtained. There are various methods of additive manufacturing depending on the process used to manufacturing the product. Stereolithography (SLA) uses liquid photopolymer resins to make desired products by selective exposure to a laser or a projector. Powder fusion is a method that includes processes such as selective laser sintering in which powdered raw material is fused and converted to solid product by exposure to high temperature lasers. Fused deposition modelling,

which is perhaps the most well-known method of additive manufacturing consist of extruding thermoplastic filaments through the printer orifice to deposit and form multi-layer products. Composites are generally manufactured using various methods, one of which is layer by layer method which is very similar to AM. AM is an ideal method for manufacturing such layer by layer composites. It may include processes ranging from hand lay-up, wet lay-up of prepreg materials, or automated fiber placement (AFP) [35-37]. All of these processes of composite manufacturing are by definition additive in nature, because they include producing the final composite part layer by layer [38-39]. AM can be helpful for the preparation of fiber reinforced polymer composites. This technology is in its initial stages when it comes to being used for the production of composites, but AM industry is fast approaching a point where its impact on the composites industry as a whole will soon become widely significant and irreplaceable [40].

Thermoplastic materials have been used to make 3D printed materials for decades due to their manageable melting temperatures as well as quick cooling times which allow for the process of 3D printing [41]. High-performance polymer filaments and other 3D printed polymer products via additive manufacturing are increasingly used due to their increased accessibility and good performances [42]. Although new materials that are not thermoplastics such as titanium, carbon fiber, and wood are being used for additive manufacturing, using thermoplastic polymers is still the most popular method. ABS used in tandem with other polymers such as nylon-6, polylactic acid and high impact polystyrene still dominate the field with the majority of the 3D printed polymer products being made using ABS hybrid polymer [43-47].

Nylon-6 is a semi-crystalline thermoplastic with good abrasion and chemical resistant properties which makes it a good candidate for AM as well as durable for engineering applications such as tire reinforcements. Other than that, it is easy to process due to its medium melt viscosity

and can be 3D-printed because of good extrusion properties which makes it an ideal candidate for studying self-healing properties because it is a sturdy material which can be 3D printed, as well as self-healed [48-50]. PLA is another polymer that has wide applications as a bulk polymer used for self-healing applications. PLA is biodegradable and non-toxic. PLA has good biocompatibility, which makes it useful for medical applications as well. Other than that, it has excellent properties after 3D printing and self-healing properties as well thus making it a genuine contender for self-healing studies [51-54].

High impact polystyrene (HIPS) is a low-cost polymer with properties leading to easy machining and fabrication. It has low strength structural application but high impact strength thus making it useful when low-cost impact strength, machinability, and fabrication are required in a product. Due to high dimensional stability, ability to be 3D printed, and ease of painting/ gluing. it is mostly used as a pre-production prototype. As a 3D printing material, HIPS has various advantages. It is an extremely low-cost material and can therefore be used for large scale additive manufacturing. The impact and water resistance of the HIPS polymer is better than most other 3D printing materials. It is also extremely lightweight and can be used as a support material in complex 3D printing jobs. It does however have certain shortcomings. Since it has a high heat resistance due to its high melting point, a heated printing bed and chamber is required. It also requires the application of glue sticks and PET tapes to avoid sticking the print bed. The 3D printing temperature is also considerably higher [55-56].

The concept of 3D printing self-healing materials is still relatively new and has not been explored extensively. Two known studies have usefully 3D printed materials that were able to autonomously heal themselves. 3D structures with in-built interconnected microvascular networks were studied and synthesized more than a decade ago using direct-ink writing. Self-healing in the

materials was achieved by delivering self-healing agent to the cracks via 3D printed microvascular network [57-60]. More recently, self-healing properties were achieved in Vinyl-terminated polydimethylsiloxane (an elastomer) using photopolymerization based additive manufacturing (stereolithography) by Yu et al. [61].

This project aims to synthesize a self-healing polymer composite by using a polymer that can be 3D printed and integrating solvent-filled microcapsules into the composite structure. The healing properties of the microcapsules are then quantified. The effects of microcapsule concentration, and healing time are studied to determine the optimum conditions required for healing. The intended outcome will be the creation of microcapsules that can survive the harsh additive manufacturing process and still provide healing to the end product.

2. Materials and Methods

2.1 Preparation of PU/UF microcapsules with EPA core fluid

Polyurethane-poly(urea-formaldehyde) (PU/UF) double-walled microcapsules containing EPA were synthesized in the laboratory using in situ polymerization of urea and formaldehyde. This method met the various criteria required for successful usage in self-healing material systems [20] such as isolation of the preferred healing liquid from the surrounding polymer to protect it from the process of additive manufacturing, excellent bonding properties to the matrix material, as well as excellent rupture and release of the healing material inside the crack plane when an external force triggers matrix damage [1][4].

The integration of microcapsules into the bulk polymer requires a few considerations. Unlike a normal synthesis process, where only the properties of the end product have to be addressed, additional care is needed to ensure the survival of microcapsules. This includes a proper choice of chemicals for the synthesis to ensure that they do not react with the microcapsule wall or its contents. Care should also be taken during mechanical agitation so that the microcapsule walls are not damaged. A suitable reaction temperature must also be maintained so that the microcapsules are not denatured before the integration are still viable. Additionally, since the end goal of this project is to manufacture self-healing materials via additive manufacturing, it is critically important that the microcapsules survive the adverse conditions of the additive manufacturing process such as high temperature and high shearing conditions.

2.2 Microcapsules synthesis

2.5 wt.% of poly (ethylene-alt-maleic anhydride) (EMA) in water was prepared by adding 3.75 g of EMA in 150 ml of water and stirring for 24 hours. After the solution was fully dissolved, 5 g urea, 0.5 g ammonium chloride and 0.5 g resorcinol (VWR chemicals) were added to the solution. 3g of PU -Desmodur L-75 (Covestro) was dissolved in 20 ml of dichloromethane (VWR) in a water bath maintained at 80 °C and added to the urea solution. The pH was maintained between 2.5 to 3 using sodium hydroxide solution. 60 ml of ethyl phenylacetate (EPA) (Sigma-Aldrich) was slowly added to the solution, and it was stirred continuously. Finally, 12.7 g of formaldehyde 37% (Alfa-Aesar) in aqueous solution was added. The reaction batch was then heated up to 55 °C, and the temperature maintained for 2 hours. 200 ml distilled water was then added to the solution to ensure that the proper emulsion of the microcapsules was maintained, and the microcapsules were heated for two more hours. Finally, the batch was cooled to room temperature, and the microcapsules were separated using filter paper. The separated microcapsules were then washed using 200 ml of water and isolated using a vacuum filter. They were then dried for 24 hours in vacuum. The microcapsules were sorted according to their sizes using a mechanical shaker and the microcapsule batch of size 200 μm was used throughout the project [17-18].

2.3 Preparation of polymer composites

Thermoplastics with high durability and multiple end-use applications were needed for this project, therefore three such thermoplastics were considered and analyzed for their compatibility with self-healing microcapsules, nylon-6, polylactic acid (PLA) and high impact polystyrene (HIPS). The methodologies for preparations of samples of each material are discussed below.

2.4 Preparation of Nylon-6 specimens

Two methods were used to prepare nylon-6 specimens; solution casting and monomer casting. Solution method is generally used for casting films. In this method, nylon-6 pellets were dissolved in a formic acid solution (Sigma-Aldrich) and poured in aluminum molds. Formic acid evaporates in 24 hours leaving behind a nylon-6 residue in shape of the mold. As seen in Figure 2.1, we get a nylon-6 sample after solvent has evaporated.

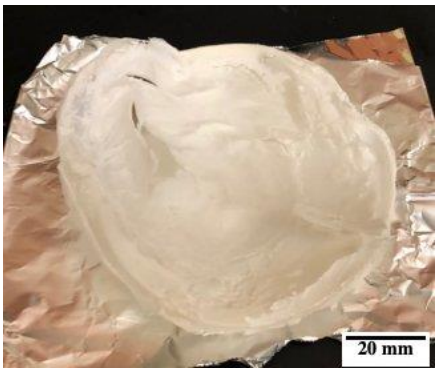

Figure 2.1 Solvent cast Nylon-6 sample

In monomer casting method, the caprolactam monomer (Sigma-Aldrich) is anionically polymerized by heating. 400 g of caprolactam monomer was heated to 80 °C. After maintaining the melted monomer at the temperature for 30 minutes, 0.6 g of sodium hydroxide (VWR chemicals) was added. Then the temperature was raised to 170 °C and toluene-2,4-diisocyanate (TDI) was added to the mixture. The solution was heated for one hour before pouring it into a stainless-steel mold. Similarly, for integration of microcapsules, 10% w/w microcapsules were added to the solution after the addition of TDI at 170 °C.

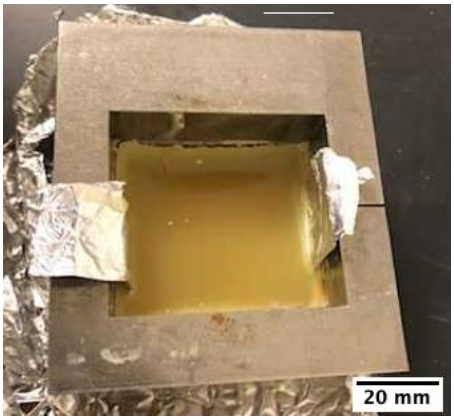

Figure 2.2 Nylon 6 monomer casting in a mold

2.5 Preparation of Polylactic acid (PLA) specimens

For PLA melt casting, 1 g of PLA pellets were placed in an aluminum mold. 2% w/w of PU/UF EPA microcapsules (0.2 g) were added and evenly mixed. The mixture was heated using a hot plate at approximately 250 °C only, to prevent deterioration of the microcapsules. Once the mixture was fully melted, the mold was removed from the hot plate and allowed to cool down. Another method was used to for microcapsule integration in the PLA sample as discussed further.

A second method to incorporate the microcapsules into PLA involved adding 100 ml of tetrahydrofuran in a beaker. 7 g of PLA pellets were added to it. The mixture was stirred using a magnetic stirrer for 2 hours until the pellets were dissolved entirely. 1 g of microcapsules was added to the solution and the solution was stirred until a uniform distribution of microcapsules was obtained. Once the microcapsules were fully dispersed another 1 g of PLA pellets was added and then after quick stirring the entire mixture was filtered out using a metal sieve. The microcapsule-coated pellets were then used for melt casting as described previously.

a) 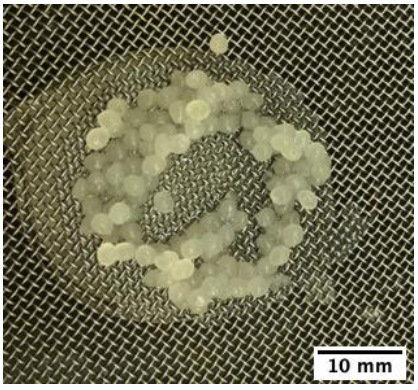

b) 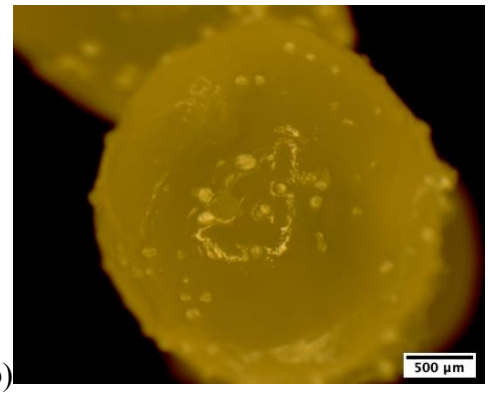

Figure 2.3 Microcapsule-coated PLA pellets a) Pellets after sieving b) Optical microscope images of a microcapsule-coated pellet

2.6 Preparation of High impact polystyrene (HIPS) samples

A combination of solvent casting and melt casting was used to integrate the microcapsules into the bulk polymer. Solvent casting was used to prepare microcapsule-integrated polymer sheets, and then compression molding was used to produce the final product of HIPS with embedded microcapsules. A stainless-steel mold was used for the compression molding of the samples. The samples were heating up to 180 °C and the temperature was maintained for 5 mins to allow the pellets to fully melt before applying pressure using the compression molding machine. The pressure was then maintained, and the samples were allowed to cool overnight.

7 g of high impact polystyrene (HIPS) pellets were placed in a beaker along with 100 ml of Tetrahydrofuran. The solution was stirred until the HIPS pellets were fully dissolved. 20% w/w of microcapsules (1.4 g) was added to the solution and thoroughly mixed. After a uniform distribution of the microcapsules was attained, the solution was poured into aluminum molds and allowed to air dry for 48 hours. The resulting polymer sheets containing the microcapsules were then used in the melt casting process.

For compression molding, a layer of HIPS pellets was placed in a stainless-steel mold. A cut out of the HIPS-microcapsule sheet obtained via solvent casting was placed on top of the layer, and some more pellets were added on top of the sheet. The mold was placed in a compression molding machine and the temperature was held at 180 °C for 5 minutes in a closed mold. After the HIPS-microcapsule mixture was fully melted, the mold was removed from the hot plate and allowed to cool to room temperature.

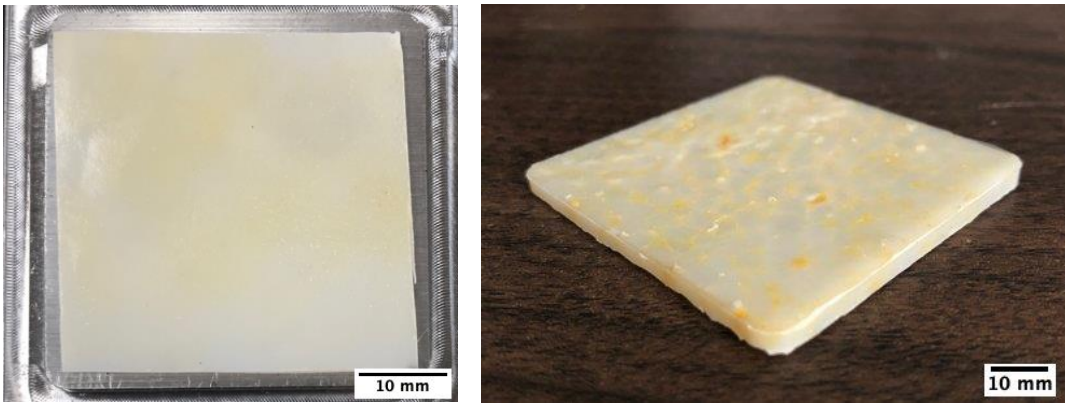

Figure 2.4 HIPS sheet made via solvent casting and finished specimen after compression molding

Another approach to incorporate microcapsules in HIPS involved adding the microcapsules directly adding the microcapsules to the batch of pellets placed in the specimen mold. The advantage of this method is that the number of microcapsules could be varied. Four batches with 3.5%, 5%, 7.5% and 10% w/w microcapsules were created. Mechanical test specimens were then cut from these microcapsule-loaded HIPS plates using an Isomet 2000 precision cutter. Each plate was cut into five equal sized piece of dimensions 50 x 10 x 2.55 mm.

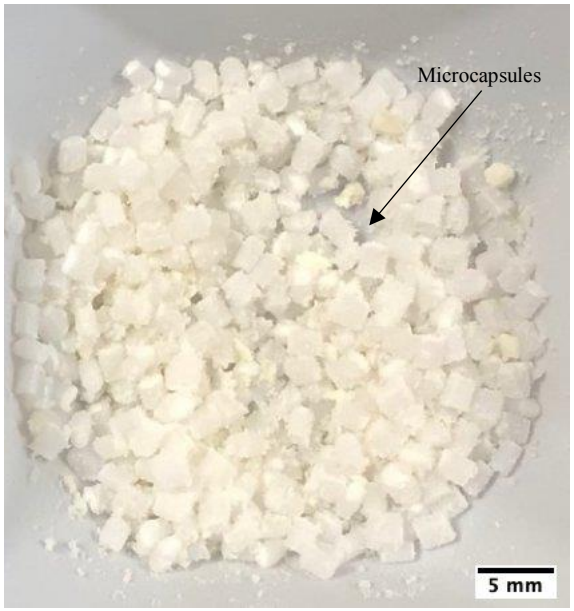

Figure 2.5 HIPS pellets EPA microcapsules mixed in before compression molding

2.7 Preparation of High impact polystyrene (HIPS) filaments

For 3D printing applications, HIPS filaments were needed. An Automatik^{Tm} polymer extruder was used to convert HIPS pellets to filaments which can be 3D printed. The zone 1 and the zone 2 temperatures were both set at 195 °C. Thus, due to heat absorption, the extruder temperature reached a temperature of 171 °C. This temperature was ideal for extruding HIPS polymer. The extruder rotation rate was maintained between 15-20 rpm to give out HIPS filaments of 0.91 mm thickness. HIPS pellets with varying concentrations of microcapsules were prepared similar to the compression molding process before being fed to the extruder.

a) 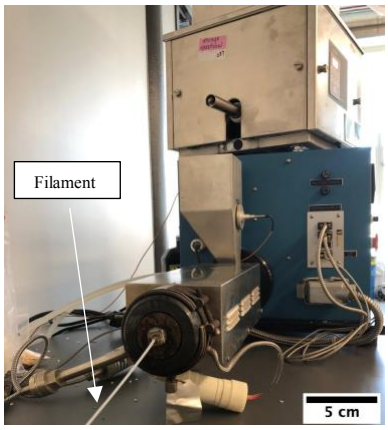

b) 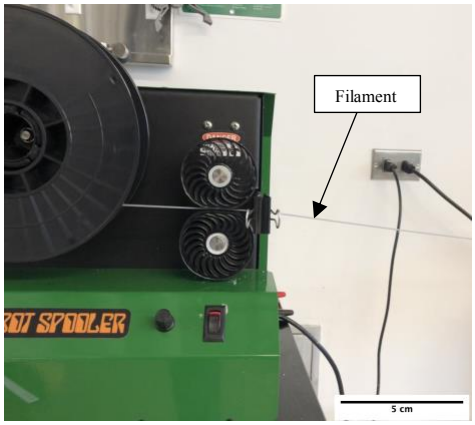

Figure 2.6 a) HIPS filament coming out of the extruder b) Spooler collecting the HIPS filament

The HIPS filament extruded from the extruder machine was collected by a spooling mechanism that was kept at a distance of 1m from the extruder to allow for proper cooling of the HIPS filament before spooling as seen from Figure 2.6

2.8 Polymer Characterization

a) After the preparations of the polymer samples, tests were performed to evaluate the quality of the resulting polymer samples and the survivability of the microcapsules. Thermogravimetric analysis (TGA) was conducted on the specimens to test the number of microcapsules in the specimens and to confirm the presence of microcapsules in the finished samples. Differential scanning calorimetry (DSC) analysis was performed to analyze the changes in thermal properties of the polymer specimens after integration of the microcapsules.

b) Dynamic mechanical analysis (DMA) tests were also conducted to characterize the thermomechanical behavior of microcapsule-load HIPS as a function of microcapsule concentration. In the DMA technique, a small deformation is applied to the sample (sample can be subjected to controlled stress or controlled strain conditions) in a cyclic manner and its response at various conditions is documented. The storage modulus (E'), as well as the glass transition

temperature (T_g) of the HIPS samples were calculated based on the DMA results. The *E'* for each microcapsule concentration is the storage modulus at ambient temperatures and a frequency of 1 Hz. T_g was obtained as the temperature value at which tan delta peaks.

2.9 Mechanical characterization

Flexure test

Flexural tests, specifically three-point bending tests were performed as per ASTM D790 on the HIPS specimens using a strain-controlled flexure testing machine (model: Instron 5565). The machine was equipped with a 5 kN load cell and a testing rate of 3 mm/min was used. HIPS samples of dimensions 50 x 10 x 2.55 mm were used for the test.

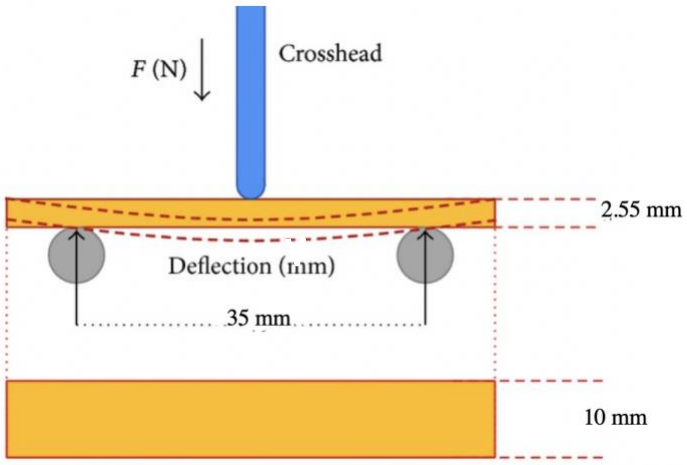

Figure 2.7 Three-point bending test to measure flexural strength and Modulus

Once completed, the values obtained for load vs. extension were obtained which were used to calculate the values of Flexural Stress (σ_f) and Flexural strain (ε_f) using the formulae

$$\sigma_f = \frac{3FL}{2bd^2} \quad [1]$$

where σ_f is the stress in the outer fibers at midpoint (Mpa), F is load at a given point on the load-deflection curve (N), L is support span (mm), b is width of beam tested (mm), and d is depth of beam tested (mm).

$$\varepsilon_f = \frac{Dd}{L^2} \quad [2]$$

where ε_f strain in the outer surface, mm/mm, D is the maximum deflection at the center of the beam (mm), L is the support span (mm), and d is the depth of the beam tested (mm).

A plot of Flexural Stress (σ_f) vs. Flexural strain (ε_f) was plotted to determine the mechanical parameters of the microcapsule-loaded HIPS, such as flexural modulus, flexural strength, and yield strength of the HIPS samples and examine the effects of the microcapsules on material properties after 48 hours and 7 days.

Fracture test

The fracture toughness, and the self-healing efficiency of the microcapsule-loaded material were evaluated using the single-edged notched beam (SENB) test. A strain-controlled flexure testing machine (model: Instron 5565) with a loading cell of 5 kN and a testing rate of 10 mm/min was used. HIPS samples of dimensions 50 x 10 x 2.55 mm with a pre-induced notch and a natural crack were used. An initial crack length of 4.5 mm was used corresponding to an approximate a/W value of 0.5. Using this a/W value (where a is the length of the crack and W is the width of the specimen, the value of f(x) is calculated using the formula

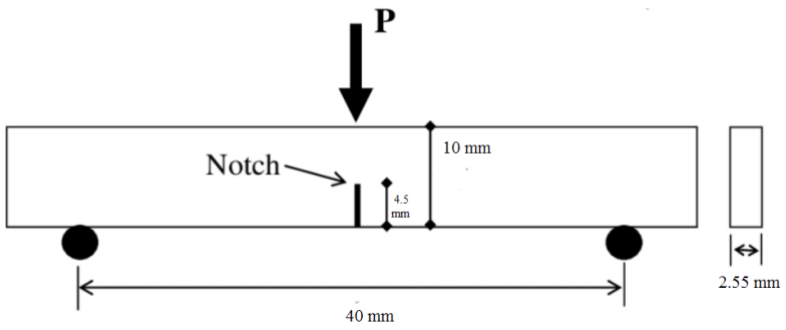

Figure 2.8 Three-point bending test to measure flexural strength

$$f(x) = 6x^{1/2}\frac{[1.99-x(1-x)(2.15-3.93+2.7x^2)]}{(1+2x)(1-x)^{3/2}} \quad [3]$$

Once we got the value of *f(x)* the value of P_Q was calculated using a 5% slope reciprocal offset and the load vs. extension plot of the specimen. Then, fracture toughness (K_Q) of the specimen was calculated using the formula

$$K_Q = \left(\frac{P_Q}{BW^{\frac{1}{2}}}\right) f(x) \quad [4]$$

where, K_Q is the Fracture toughness, P_Q is the Offset intercept, B is the Specimen thickness, and W is the Specimen width.

2.10 Imaging

The size of the microcapsules, the presence of self-healing fluid, the distribution of microcapsules in the polymer specimen, and the integrity of microcapsules after the compression molding process were all examined via optical microscope. Scanning electron microscopy (SEM) was also used to obtain higher quality images of the microcapsules as well as to confirm microcapsule compatibility with the host polymer by inspecting the microcapsule-polymer

interface. Zeiss EVO50 Scanning Electron Microscope was used for obtaining high quality microscopic images of the sample structure as well as the microcapsules in the bulk polymer.

3. *Results and Discussion*

3.1 Characterization PU-UF microcapsules with EPA self-healing fluid

Thermogravimetric analysis (TGA) was used to understand and analyze the thermal stability of the microcapsules that were introduced in the HIPS samples. The TGA plot for the microcapsules is shown in Figure 3.1. On the plot there is a 10% moisture loss up until a temperature of 100 °C. This weight loss is due to the microcapsules absorbing moisture and can be prevented using air-tight storage containers. After this, the capsules are thermally stable up to a temperature of 200 °C after which there is a steep reduction in the weight percent. At a temperature of approximately 245 °C, there is 30% mass loss. Using the TA universal analysis software, the onset point was calculated as shown in the graph. The onset points of 228.09 °C is approximately equal to the confirmed boiling point of EPA (229 °C). This indicates that the microcapsules undergo mass loss 200 °C to 250 °C and thus can be used to verify the presence of microcapsules in the various bulk polymer.

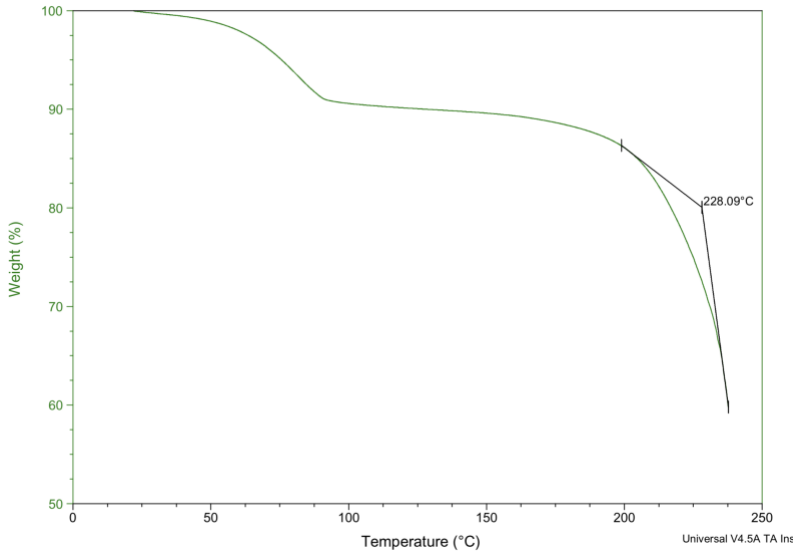

Figure 3.1 TGA of microcapsules

The DSC results of the microcapsules as shown in Figure 3.2 illustrate a number of disturbances, but no major peaks up to 230 °C. This corroborates the data obtained from TGA that the microcapsules are stable till a temperature of 230 °C. There is a major peak starting at circa 210 °C and then peaks around 230 °C. Comparing these results to those from the TGA analysis, this temperature corresponds to the boiling point of EPA, so this peak can be explained as a result of evaporation of EPA from the microcapsules. From this analysis, it can be hypothesized that an operating temperature of less than 230 °C would be optimal for ensuring that the microcapsules survive the AM process.

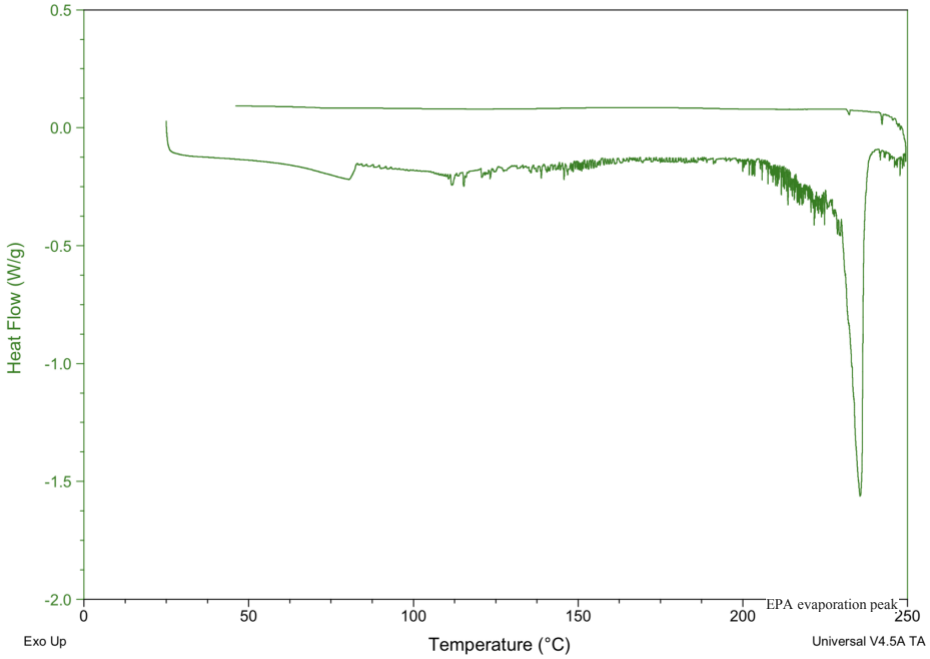

Figure 3.2 DSC reading of microcapsules

3.2 Nylon-6

The solvent-cast nylon-6 samples were flaky and highly brittle, see Figure 2.1. Therefore, they were not suitable for our investigations. The monomer casted samples were of a better quality, however. Comparative thermo-gravimetric analysis (TGA) of virgin samples and nylon-6 samples with microcapsules produced during monomer casting were performed.

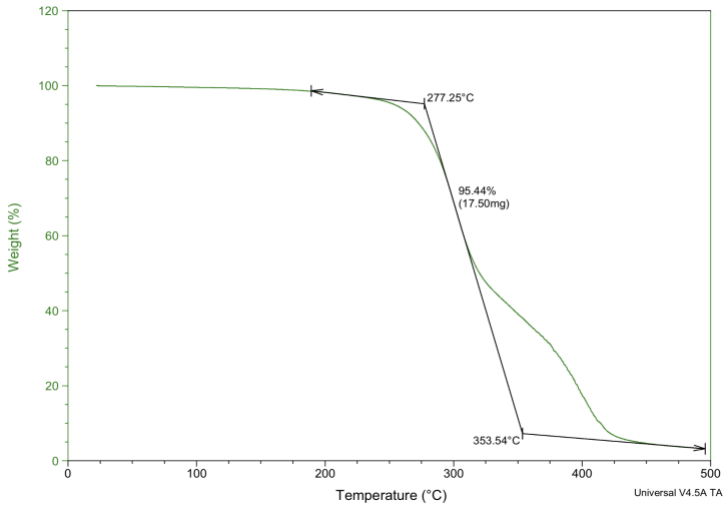

Figure 3.3 Thermogravimetric analysis (TGA) of monomer cast Nylon-6 sample

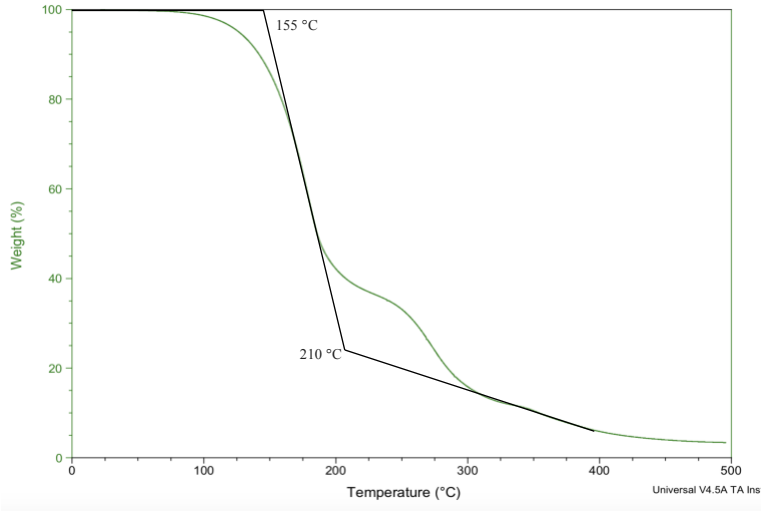

Figure 3.4 TGA of EPA microcapsule integrated Nylon-6 sample

As illustrated in Figure 3.3 and Figure 3.4, the virgin nylon-6 sample is approximately 95% pure and shows great thermal stability up to a high temperature of 277 °C as seen from the flat and stable plot. But the microcapsule integrated specimen however has inferior thermal stability and begins degrading at a significantly low temperature of 110 °C. Approximately 60% of the sample is degraded before reaching a temperature of 200 °C. These temperatures coincide with the melting point of the monomer, i.e. Caprolactam, and indicates that a vast majority of the monomer is still unreacted. A possible reason for unreacted monomer being present is because the nylon-6

polymerization reaction requires basic conditions, but the pH has possibly been changed due to the addition of acidic microcapsules. The acidity of microcapsules was confirmed using a pH paper during the synthesis process. It was then decided not to pursue nylon-6 as a candidate for incorporating EPA microcapsules.

3.3 Polylactic Acid (PLA)

The PLA samples as seen in Figure 3.5, showed great microcapsule dispersion; however, they were not soluble in EPA, see Figure 3.6 because the solubility parameters of PLA(20.3) and EPA (7.2) are too far apart. As a result, PLA will not undergo solvent based self-healing, when the microcapsules are ruptured during damage. No further analysis was performed on the PLA microcapsule system.

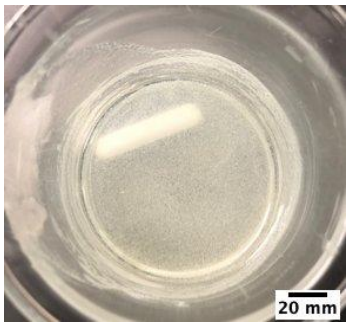

Figure 3.5 EPA microcapsules distributed in PLA ink

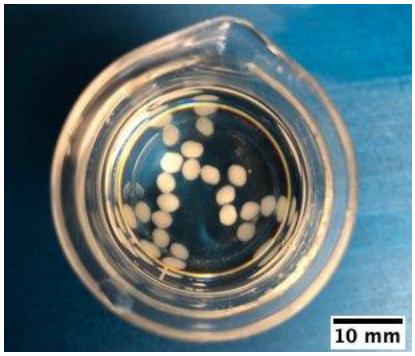

Figure 3.6 PLA pellets in EPA liquid after 2 hours of immersion (Note that the PLA pellets do not dissolve)

3.4 High-impact polystyrene (HIPS)

HIPS however is a polymer that is compatible with the self-healing fluid (EPA) as shown in Figure 3.7 where two HIPS pellets are bonded together by a drop of EPA. This is because solubility parameter of HIPS (~8) is close to solubility parameter of EPA (7.2)

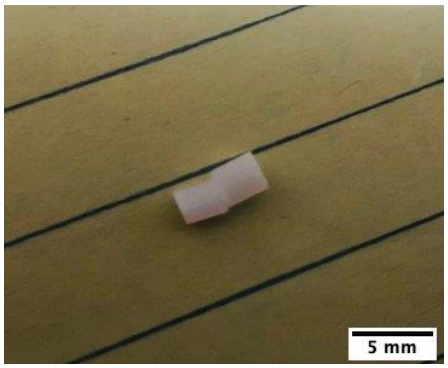

Figure 3.7 Two HIPS pellets joined by a drop of EPA

Microscopy analysis

As seen from Figure 3.8, the cross-section of a melt cast of HIPS with embedded microcapsules. Intact microcapsules within the phase of the bulk polymer are clearly visible. Further thermomechanical testing was performed to confirm the integrity of the microcapsules.

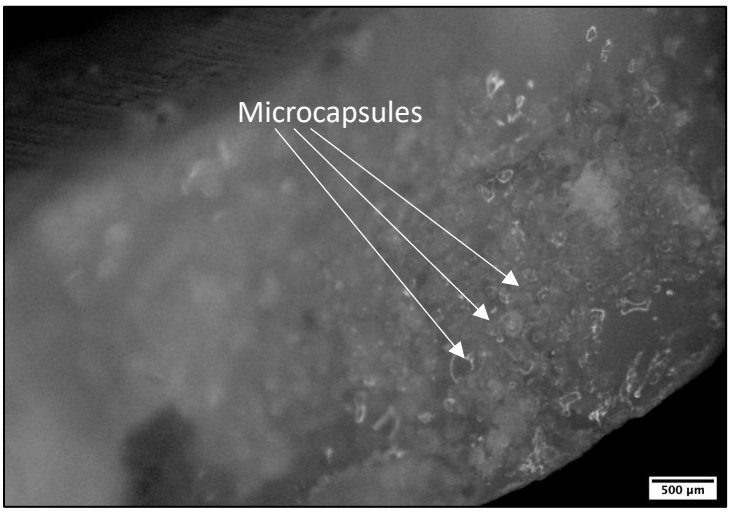

Figure 3.8 Cross-section of HIPS polymer specimen with EPA microcapsules

Thermal analysis using DSC

As seen from Figure 3.9 and Figure 3.10 of the polymer sample with the integrated microcapsules and the polymer sample without integrated microcapsules, there are no noticeable changes in the graphs. Thus, it can be said that the addition of microcapsules only affects the maximum heat flow of the samples. Which means, while the T_g of the samples remain unchanged, the sample with embedded EPA microcapsules needed slightly more heat energy to reach the same temperature.

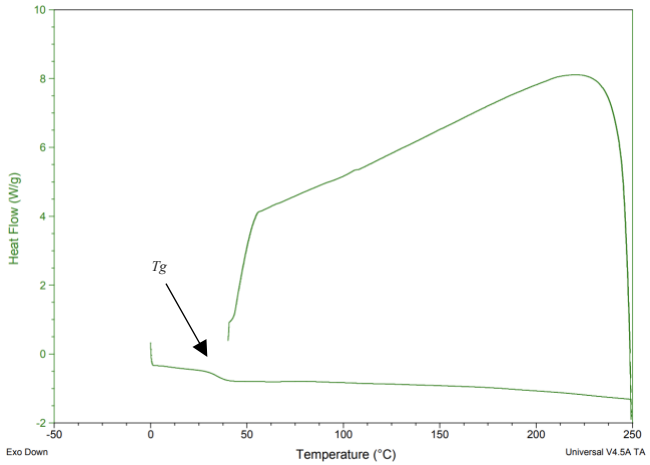

Figure 3.9 DSC plot of HIPS specimen with embedded EPA microcapsules

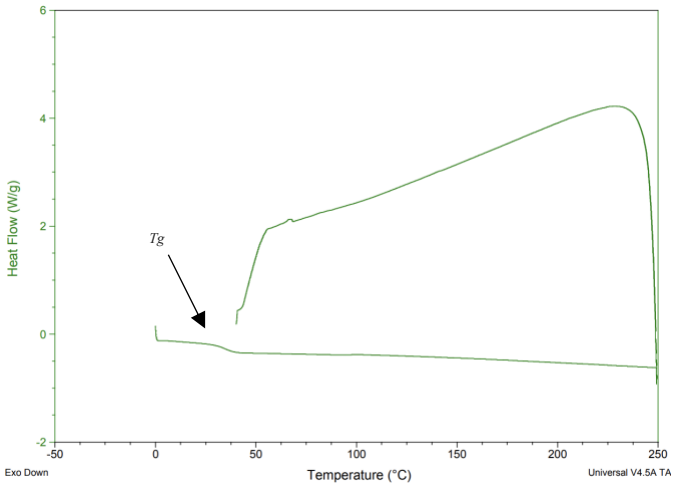

Figure 3.10 DSC plot of HIPS specimen without microcapsule

Microcapsule survivability test

A solvent filtration method was used to determine whether the microcapsules had maintained their structural integrity and self-healing components after the compression molding process. A conical filter paper was placed over the mouth of the beaker filled with 250 ml of THF. Chunks of the finished samples were added to the THF in such a way that the THF was not directly in contact with the HIPS sample but instead was allowed to soak through the filter paper to dissolve HIPS. After one hour, when the HIPS sample was fully dissolved, the contents of the filter paper (dissolved sample + THF) were emptied onto a metal micro-sieve as shown in Figure.

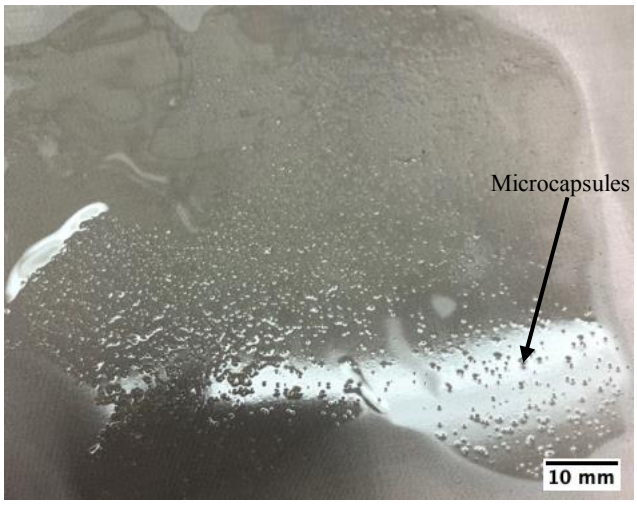

Figure 3.11 EPA microcapsules after HIPS specimen is dissolved using tetrahydrofuran

The metal sieve was then dried in an oven at 80 °C for an hour to evaporate the residual solvent. Once it was completely dried, the metal sieve was analyzed under a microscope to identify the microcapsules that remained, see Figure 3.12.

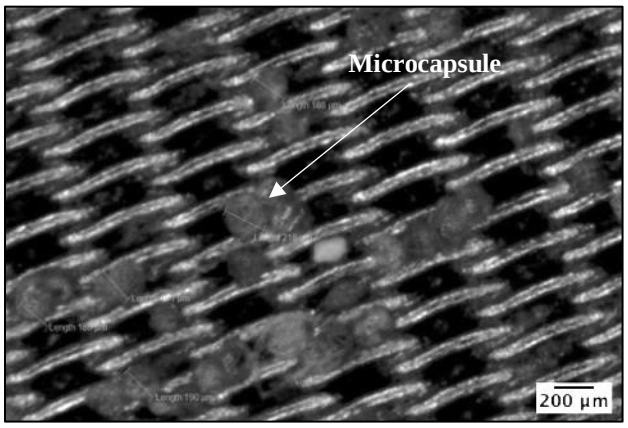

Figure 3.12 Microscopic image of EPA microcapsules obtained by solvent filtration of samples of HIPS embedded with microcapsules

After the microscopic analysis, the presence of self-healing fluid in the capsules was verified. The microcapsules were removed from the metal sieves and crushed between two glass slides. The crushed microcapsules were inspected under the microscope again to detect the presence of any leaked self-healing fluid, see Figure 3.13.

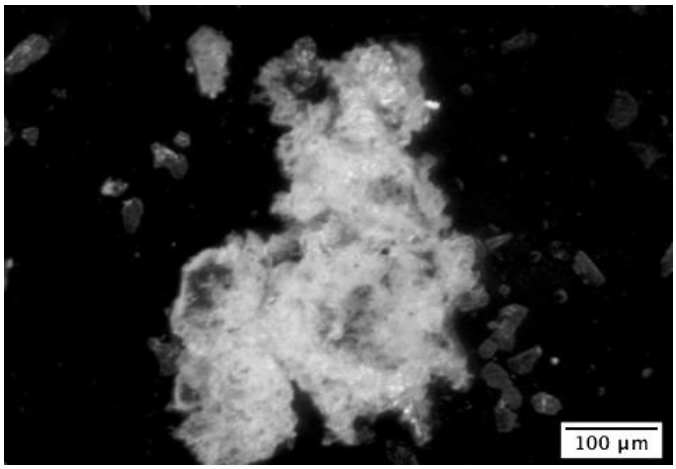

Figure 3.13 Microscopic images of crushed EPA microcapsule

Comparative TGA analysis of HIPS samples with embedded EPA microcapsules.

From the comparative TGA analysis in Figure 3.14 the TGA plot for the sample with no microcapsules is flat and stable up to 400 °C. In the TGA plots for samples with microcapsules, however, it is observed that there is a significant weight loss beginning around 170 °C and becoming steeper around 229 °C, which is the boiling point of EPA. A cleaner picture of the mass drop was obtained by performing TGA tests up to 250 °C.

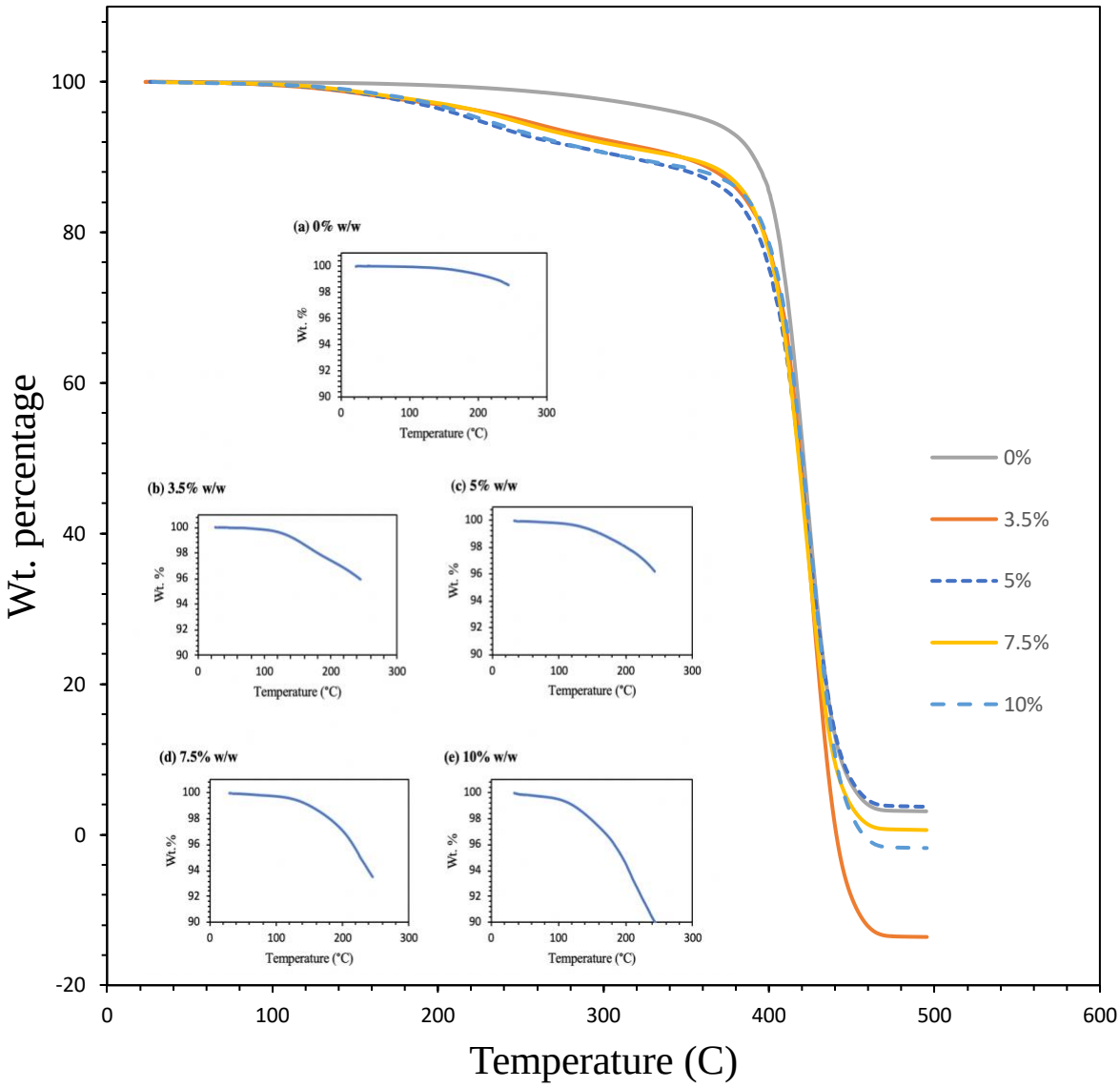

Figure 3.14 Comparative TGA data for different microcapsule concentration

As seen from Figure 3.14 (a), the HIPS sample with no microcapsules is highly stable at the temperature of 250°C. There is no weight loss up to a temperature of approximately 150 °C and after that less than 2% weight loss by the time the temperature reaches 250 °C.

In the Figure 3.14 (b), the effect of adding 3.5% w/w microcapsules on the HIPS sample is visible. The sample is relatively stable but starts losing a greater weight as compared to the previous sample due to the presence of microcapsules. There is approximately 4% weight loss by the time the sample reaches the temperature of 250 °C which can be explained by the evaporation of EPA in the microcapsules.

In Figure 3.14 (c), the HIPS sample with 5% microcapsule content was tested. Not unlike the previous graph, the sample is stable up to a temperature of approximately 120 °C. From that point, there is a weight loss of approximately 4% by the time the temperature is 250 °C. On comparing this sample with the previous sample, it can be observed that they have a similar graph because of almost identical weight percentages of microcapsules in them.

In Figure 3.14 (d), it can be seen the TGA graph for HIPS sample with 7.5% microcapsule content. As observed from the graph, the weight drop is significant compared to the previous two samples. The weight loss starts from approximately 100 °C, and as the temperature reaches 250 °C there is a weight loss of approximately 7%, which roughly corresponds with the weight percentage of the microcapsules in the HIPS sample.

In Figure 3.14 (e), it can be observed is the TGA of HIPS sample with 10% microcapsule content. After being stable up to a temperature of 120 °C, the sample shows a weight loss of approximately 10% as the temperature reaches 250 °C. This is more than 3.5%, 5%, and the 7.5% sample. Just like the weight loss of the 7.5% sample corresponded roughly with the number of capsules in the HIPS sample, a more significant weight loss in 10% HIPS sample is observed,

which suggests that we have obtained the required wt% of the microcapsules in the HIPS specimens.

Dynamic Mechanical Analysis (DMA)

MC conc. (%w/w)	Storage Modulus (*E'*) (MPa)	Glass Transition Temperature (T_g) (°C)
0	1225.8	110.6
3.5	807.2	100.4
5	1008.4	104.4
7.5	1011.7	98

Table 3.2 Changes in storage modulus and glass transition temperature of HIPS specimens with change in microcapsule concentration

With the help of DMA, the effect of the addition of microcapsule on the storage modulus (*E'*) and the glass transition temperature (T_g) was determined. A seen from Table 3.2, the storage modulus does not show any fixed trend, but the addition of microcapsules slightly lowers the storage modulus of the HIPS specimens. Similarly, it is seen that the glass transition temperatures of the HIPS specimens also decrease with the increase in the microcapsule concentration.

Scanning Electron Microscopy (SEM)

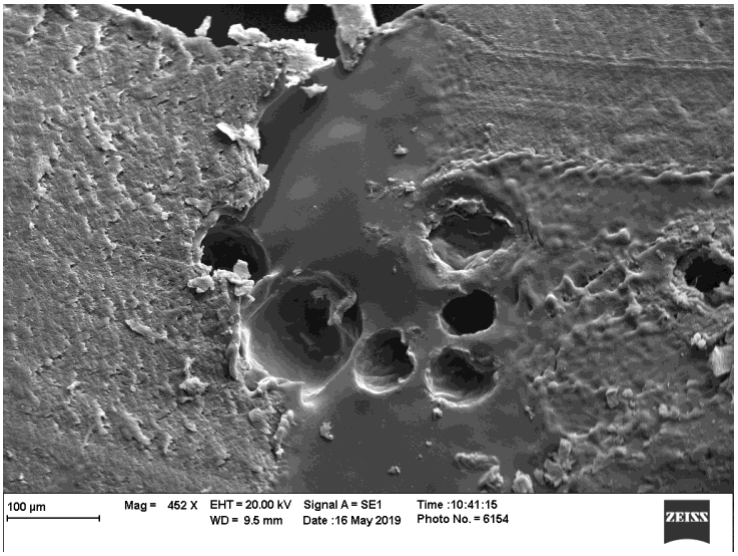

Figure 3.15 Microcapsule cavities in a 5% w/w HIPS sample

Zeiss EVO50 Scanning Electron Microscope was used for taking this magnified image of a HIPS sample with 5% w/w microcapsules. In Figure 3.15 we can see the cavities where the microcapsules were embedded. The smooth, almost spherical shape of the cavities left behind by the microcapsules suggests that the microcapsules show good bonding with the bulk polymer. The reason however, that the microcapsules are missing from this image may be due to the shear forces exerted on the polymer by the mechanical saw used to cut the HIPS sample. Therefore, in order to observe the microcapsules inside the bulk polymer (and their interaction), microcapsules embedded in HIPS sheet was observed using SEM.

Flexure testing analysis

As seen from Figure 3.16, the virgin HIPS samples had the highest flexural modulus. The addition of microcapsules causes a somewhat steady decrease in the flexural modulus of the sample. The flexure strength follows the same trend shown by the flexure modulus as seen in fig 3.17

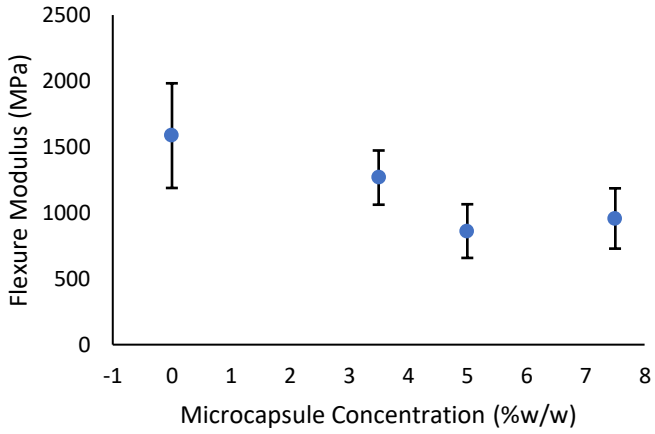

Figure 3.16 Effect of microcapsule concentration on flexural modulus of HIPS

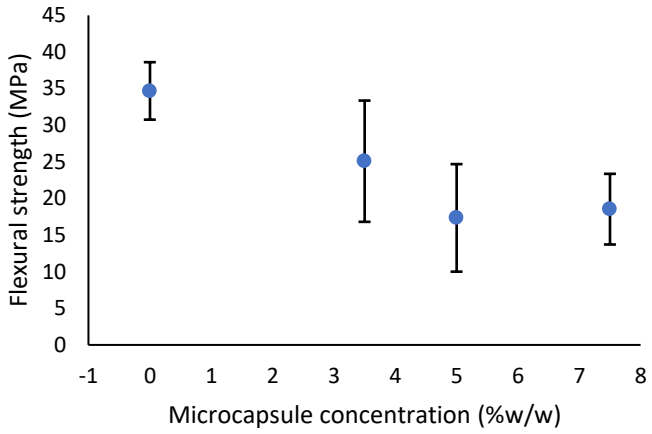

Figure 3.17 Effect of microcapsule concentration on maximum strength of HIPS

Fracture testing analysis

As seen from table 3.1, the maximum fracture toughness value of the HIPS specimens decreases with the increase in the concentration of microcapsules. But, as seen from the fracture toughness value after the specimens were allowed to heal for 48 hours, the effects of microcapsules are clearly visible. The 3.5% and 5% specimens both show good fracture toughness recovery and it can be said that after 48 hours, 3.5% w/w offers optimal self-healing properties as seen from Figure 3.18

Similarly, from Table 3.1 we can also see the effects of the increase in the microcapsule concentration on the fracture toughness after allowing the samples to heal for 7 days. As expected, the percentage recovery of the fracture toughness increases with increase in the concentration of microcapsules with 5% w/w showing the lowest and 7.5% w/w specimens showing the highest percentage recovery as seen from Figure 3.18. Thus, it can be observed that for the higher microcapsule concentrations to show better recovery, more healing time is needed.

Table 3.1 Fracture toughness before and after healing as a function of microcapsule concentration after 48 hours and 7 days

MC Conc. (%w/w)	Pre-healing Fracture Toughness ($MPa.m^{1/2}$)	Post Healing Fracture Toughness (48 hours) ($MPa.m^{1/2}$)	% Recovery (%)	Post Healing Fracture Toughness (7 days) ($MPa.m^{1/2}$)	% Recovery (%)
0	1652.1 ± 366	-	-	-	-
3.5	1334.1 ± 465	1197.8 ± 405	89.8	627.9 ± 300	47
5	1256.9 ± 333	1019.1 ± 327	81.1	736.3 ± 280	58.5
7.5	1259.2 ± 546	745.8 ± 251	59.3	785.6 ± 353	62.3

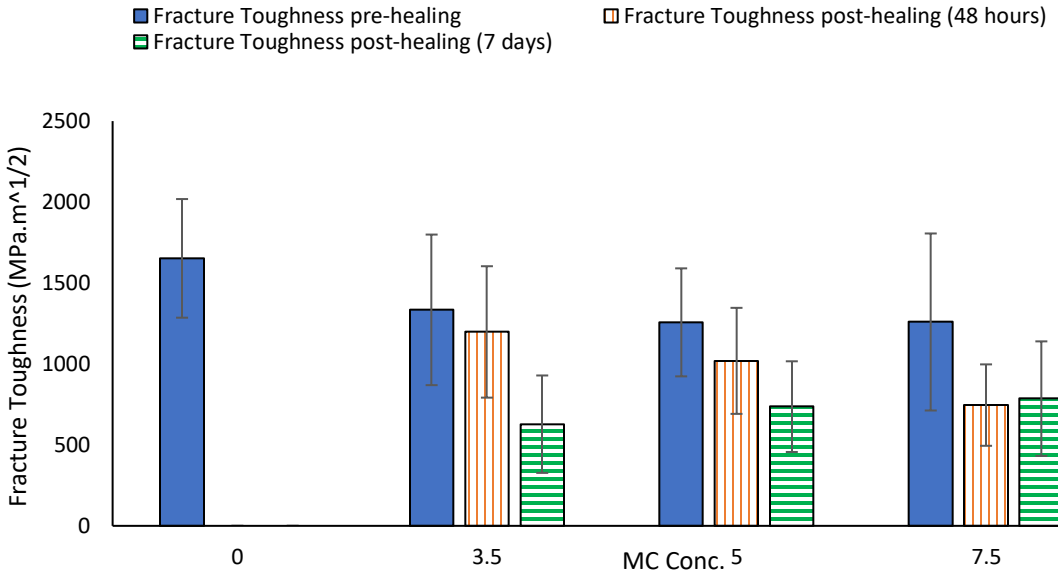

Figure 3.18 Fracture toughness before and after healing as a function of microcapsule concentration after 48 hours and 7 days

HIPS filaments with microcapsules

Once the HIPS filaments with integrated microcapsules were extruded, they were allowed to dry. A cross section of the filament was observed under the microscope to confirm the survival of the capsules. As seen from Figure 3.19, there are microcapsules visible in the cross section of the filaments. But the presence of large number of voids was also noted in the microscopic image.

The filaments were later dissolved using THF and the microcapsules were isolated on a filter paper as shown in Figure 3.19. The microcapsules appear to have survived the extrusion process and further characterization of the microcapsules is needed to confirm their viability.

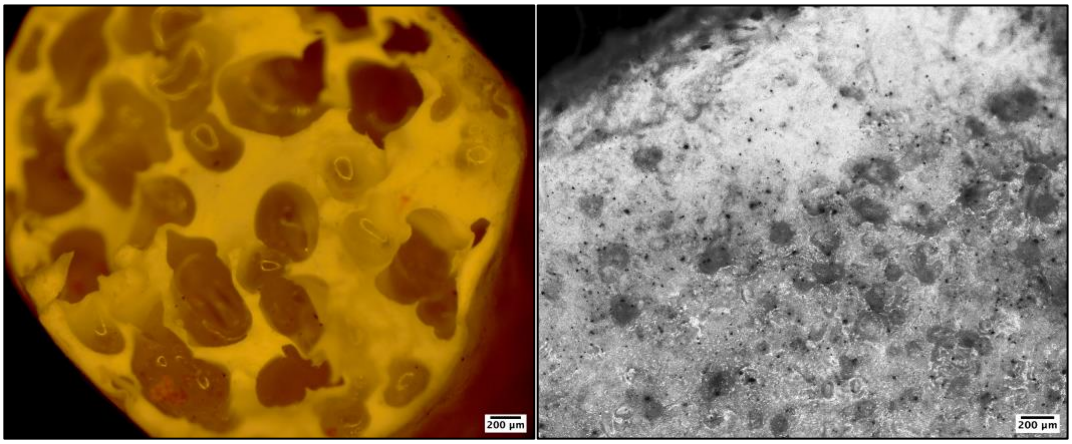

Figure 3.19 Cross section of microcapsule embedded HIPS filament and separated microcapsules

4. Conclusions and future work

4.1 Conclusions

Though nylon-6 offers good physical and thermal properties, it is not possible to integrate the PU-UF capsules during the monomer casting process due to the considerable difference in their respective pH. A potential solution is to introduce microcapsules with different chemistry and suitable pH during the nylon-6 polymerization reaction in such a way that they do not disrupt the nylon-6 polymerization process. Moreover, solution casting may be a suitable method for casting self-healing films in the future, but the technique is not suitable for creating composites and other such products.

As it stands, self-healing in PLA products cannot be achieved with the EPA microcapsules being used for this project. Since the solubility parameters of EPA and PLA are not close enough, EPA cannot dissolve PLA and thus 'Solvent based self-healing' is not possible with EPA. There are however two alternative approaches that can be explored. The first one is changing of the solvent from EPA to some other appropriate solvent which can dissolve PLA, which in turn will pave the way for self-healing. The other possible alternative is to change the self-healing system from solvent-based self-healing system to catalyst based self-healing system.

HIPS was the most promising of the three because of its positive results. The EPA drop test demonstrated that HIPS was compatible with EPA solvent for solvent-based self-healing. Preliminary microscopic tests of the cross-section of a finished HIPS product showed that the microcapsules appeared to have survived the compression molding process. The solvent filtration test confirmed that the capsules had maintained their structural integrity and shape. Crushing the microcapsules as mentioned earlier further confirmed (at least visually) that EPA, i.e. the self-healing fluid was still present in the microcapsules.

The DSC test conclusively demonstrated that the thermal properties of the HIPS polymer remain unchanged even after the addition of microcapsules. This is important because one of the aims of this project was to demonstrate that self-healing is possible via additive manufacturing, a process where the thermal properties of the polymer affect the outcome. Hence, we can say that operating temperature for additive manufacturing of a self-healing polymer can be the same as that of said polymer without the self-healing properties.

The TGA results confirm the findings of the solvent filtration test. The systematic dip in the weight of the samples around the boiling point of EPA confirms the presence of self-healing fluid in the finished sample, thus proving the viability of the self-healing microcapsules even after the compression molding process. Moreover, the increase in weight loss with the rise in the number of microcapsules in the polymer sample proves that even distribution is indeed possible.

Thus, it can be safely hypothesized that if the microcapsules can survive the high temperature, high-pressure conditions of the compression molding process, they are most likely to survive the additive manufacturing process, thus paving the way for self-healing polymer composites manufactured via additive manufacturing.

From the flexural tests, it was observed that the addition of microcapsules led to a decrease in the mechanical properties of the HIPS sample. This is because the capsules, due to their nature act as stress concentrators by introducing regions of voids in the HIPS phase. Thus, cracks and stress lines are more likely to propagate through samples which have microcapsules. Geometric discontinuities such as the added microcapsules create an increased in the intensity of the local stress fields. Increase in the local stresses can have negative effects on the mechanical properties of the samples, so care must be taken to compensate and keep this in mind before addition of microcapsules.

From the fracture tests, it was observed that addition of microcapsules decreases the maximum fracture toughness values of the HIPS specimens. As hypothesized from the flexural test results, this can be due to the microcapsules acting as stress concentrators and aiding crack propagation. In the specimens allowed to heal for 48 hours, the 3.5% w/w sample showed the most recovery. Although it was observed that for the specimens allowed to heal for 7 days, the percentage recovery of fracture toughness increased with the increase in the microcapsule concentration. Therefore, it can be hypothesized that higher concentrations of microcapsules require a longer healing time for self-healing. These results suggest that an increase in the concentration of self-healing microcapsules leads to increased self-healing and mechanical properties recovery if the healing time is longer.

The values of changes in the storage modulus (E') and glass transition temperature (T_g) of the HIPS specimens with varying concentrations was obtained from the DMA. Using the mean value and the standard deviation of all the values of both the storage modulus as well as the T_g, the coefficient of variance (CV) for both E' and T_g were calculated which are 0.17 and 0.05 respectively. Such low values of CV indicated a really low spread of data. Thus, it can be hypothesized that the addition of microcapsules has a negligible change in the storage modulus and the glass transition temperatures of the HIPS specimens.

4.2 Future work

In the future, 3D printed samples of the polymer with integrated microcapsules will be made using the microcapsule integrated HIPS filaments to prove that it is possible to have self-healing in 3D printed polymers. This project demonstrates that the capsules and its contents survive

the harsh conditions of the compression molding process, so the next step would be to perform the same series of tests on 3D printed samples containing self-healing microcapsules.

Furthermore, more testing is to be done using the compression molded specimens with more controls with both 100% and 0% healing scenarios. For example, some of the tests include testing the self-healing in virgin HIPS specimens by injecting EPA solvent directly in to the cracks to undergo self-healing. Another test includes adding DCPD filled capsules to the HIPS specimens to show lack of self-healing with the addition of Grubbs' catalyst.

Finally, the percentage recovery values of the mechanical properties of block HIPS specimens manufacture via compression molding will be compared to the 3D printed HIPS specimens to determine how the change in manufacturing method affects the rate and the percentage of self-healing.

4. References

1. White SR, et al. 2008. Autonomic healing of polymers. MRS Bull. 33(8):766–69
2. Bond IP, et. al. Self-healing fiber-reinforced polymer composites. MRS Bull. 33:770–74
3. Trask RS, et al. 2007. Self-healing polymer composites: mimicking nature to enhance performance. Bioinspiration Biomimicry. 2(1):1–9
4. B.J. Blaiszik, et al. (2010). Self-Healing Polymers and Composites. Annual Review of Materials Research Vol. 40, 179-211.
5. N. K. Guimard, et al. (2012). Current trends in the field of self-healing materials. Macromolecular Chemistry and Physics, vol. 213, no. 2, 131-143.
6. Margaret Scheiner, et al. (2016). Progress towards self-healing polymers for composite structural applications, Polymer, Volume 83, 260-282.
7. Kessler M. R., et al. (2001). Self-activated healing of delamination damage in woven composites. *Composites Part A: Applied Science and Manufacturing,* 32, 683-699
8. Kessler M. R., Sottos N. R., White S. R., Self-healing structural composite materials.*Composites Part A: Applied Science and Manufacturing,* 2003, 34, 743-753
9. Peterson, A. M. (2009). Reversible Diels–Alder cycloaddition for the design of multifunctional network polymers. John Wiley and Sons.
10. Neuser, S. et al. (2014). Fatigue response of solvent-based self-healing smart ma-terials. *Experimental Mechanics,* 54, 293-304.
11. Liu X. et al. (2009). Rheokinetic evaluation of self-healing agents polymerised by Grubbs' catalyst embedded in various thermosetting systems. *Composites Science and Technology, 69*, 2102-2107.

12. Peng, R., et al. (2014). Conductive nanocomposite hydrogels with self-healing property. *Rsc Advances*, *4*(66), 35149-35155.
13. Dai, S., et al. (2018). A self-healing conductive and stretchable aligned carbon nanotube/hydrogel composite with a sandwich structure. *Nanoscale*, *10*(41), 19360-19366.
14. Li, G. (2015). Self-Healing Composites: Shape Memory Polymer Based Structures. John Wiley and Sons.
15. A.R. Jones, et al. (2013). Full recovery of fiber/matrix interfacial bond strength using a microencapsulated solvent-based healing system. Composites Science and Technology, Volume 79, 1-7.
16. B.J. Blaiszik, et al. (2009). Microcapsules filled with reactive solutions for self-healing materials. Polymer, Volume 50, Issue 4, 990-997.
17. Caruso M. M., et al. (2008). Full recovery of fracture toughness using a nontoxic solvent-based self-healing system. *Advanced Functional Materials,* 18, 1898-1904.
18. Caruso M. M., et al. (2007). Solvent promoted self-healing epoxy materials. *Macromolecules,* 40, 8830- 8832.
19. Blaiszik BJ, et al. 2009. Microcapsules filled with reactive solutions for self-healing materials. Polymer 50(4):990–97
20. Dong Yu Zhu, et al. (2015). Self-healing polymeric materials based on microencapsulated healing agents: From design to preparation, Progress in Polymer Science, Volumes 49–50, 175-220.
21. Blaiszik BJ, et al. 2008. Nanocapsules for self-healing materials. Compos. Sci. Technol. 68(3–4):978–86

22. Benita S, et al. 2006. Microencapsulation: Methods and Industrial Applications. Boca Raton, FL: CRC/Taylor & Francis
23. Brown EN, et al. 2003. In situ poly(urea-formaldehyde) microencapsulation of dicyclopentadiene. J. Microencapsulation. 20(6):719–30
24. Asha-Dee N. Celestine, et al. (2015). Autonomic healing of PMMA via microencapsulated solvent, Polymer, Volume 69, 241-248.
25. Min Wook Lee, et al. (2018). Advances in self-healing materials based on vascular networks with mechanical self-repair characteristics. Advances in Colloid and Interface Science, Volume 252, 21-37.
26. Trask R., et al. (2006). Biomimetic self-healing of advanced composite structures using hollow glass fibres. *Smart Material and Structures*, 2006, 15, 704-710.
27. Trask R. S., et al. (2007). Bioinspired self-healing of advanced com- posite structures using hollow glass fibre*s*. *Journal of the Royal Society Interface*4, 363-371.
28. Kurman, H. L. (2013). Fabricated: The new world of 3D printing. John Wiley & Sons
29. Christian Weller, et al. (2015). Economic implications of 3D printing: Market structure models in light of additive manufacturing revisited. International Journal of Production Economics, 43-56.
30. Barry Berman. (2012). 3-D printing: The new industrial revolution, Business Horizons, 155-162.
31. Holmes, M. (2019). Additive manufacturing continues composites market growth. Reinforced Plastics.
32. Xue Yan, P. Gu. (1996). A review of rapid prototyping technologies and systems. Computer-Aided Design, Volume 28, Issue 4, 307-318.

33. W. Zhong, et al. (2001) Short fiber reinforced composites for fused deposition modeling. Mater. Sci. Eng. A 301, 125–130
34. M. Nikzad, et al. (2011). Thermo-mechanical properties of highly filled polymeric composites for fused deposition modeling. Mater. Des. 32, 3448–3456
35. Introduction to additive manufacturing for composites, (2017). Retrieved in 2019 from Stratasys.com:https://energygroup.it/getattachment/dd11d248-7452-4b60-a6b4-c075ab2dc697/Come-progettare-per-il-Direct-Digital-Manufacturin.aspx
36. Daniel-Alexander Türk, et al. (2017). Composites Part Production with Additive Manufacturing Technologies. Procedia CIRP, Volume 66, 306-311.
37. Love, L. J. (2014). The importance of carbon fiber to polymer additive manufacturing. Journal of Materials Research, 1893-1898.
38. Syed A.M. Tofail, et al. (2018). Additive manufacturing: scientific and technological challenges, market uptake and opportunities. Materials Today, 22-37.
39. Wong, K. V. (2012). A review of additive manufacturing. ISRN Mechanical Engineering.
40. Layer: S.H. Masood, et al. (2004). Development of new metal/polymer materials for rapid tooling using fused deposition modeling. Mater. Des. 25, 587–594 (2004)
41. http://www.engineering.com/3DPrinting/3DPrintingArticles/ArticleID/6262/Infographic-The-History-of-3D-Printing.asp
42. De Leon, et. al. High-performance polymer nanocomposites for additive manufacturing applications. React Funct Polym 2016103141–155
43. D. Croccolo, et al. (2013). Experimental characterization and analytical modeling of the mechanical behaviour of fused deposition processed parts made of ABS-M30. Comput. Mater. Sci. 79, 506–518

44. I. Sbarski, et al. (2009). A study of melt flow analysis of ABS–iron composite in fused deposition modeling process. Tsinghua Sci. Technol. J. 14, 29–37
45. T. Liu, et al. (2008). Melt rheological properties of nylon 6/multi-walled carbon nanotube composites. Compos. Sci. Technol. 68, 2498–2502
46. I.L. Lombardi, et al. (1997). Issues associated with EFF & FDM ceramic filled feedstock formulation, in Proceedings of Solid Freeform Symposium, University of Texas, Austin.
47. B. Caulfield, et al. (2007). Dependence of mechanical properties of polyamide components on build parameters in the SLS process, Journal of Materials Processing Technology, Volume 182, Issues 1–3, Pages 477-488, ISSN 0924-0136
48. Singh, R., et al. (2014). Development of Nylon Based FDM Filament for Rapid Tooling Application. Journal of The Institution of Engineers (India): Series C, 95(2), 103–108.
49. Singh Boparai, et al. (2016). Experimental investigations for development of Nylon6-Al-Al2O3 alternative FDM filament. Rapid Prototyping Journal, 22(2), 217–224.
50. K.S. Boparai, et al. (2016). Thermal characterization of recycled polymer for additive manufacturing applications, Composites Part B: Engineering, Volume 106, Pages 42-47
51. Aravind Raj, et al. (2018). A Case Study of 3D Printed PLA and Its Mechanical Properties, Materials Today: Proceedings, Volume 5, Issue 5, Part 2, Pages 11219-11226
52. Kuentz Lily, et al. (2017). Additive manufacturing & Characterisation of Polylactic acid composites containing metal reinforcements National Aeronautics and space administration
53. P Aveen, et al. (2018). 3D Printing & Mechanical Characterisation of Polylactic Acid and Bronze Filled Polylactic Acid Components. IOP Conference Series: Materials Science and Engineering. 376. 012042. 10.1088/1757-899X/376/1/012042.

54. B.M. Tymrak, et al. (2014). Mechanical properties of components fabricated with open-source 3-D printers under realistic environmental conditions, Materials & Design, Volume 58, 2014, Pages 242-246

55. Singh, R., et al. (2019). Multi-Material Additive Manufacturing of Sustainable Innovative Materials and Structures. Polymers, 11(1), 62.

56. Kumar, R. et al. (2018). On the multi-material 3D printing of recycled ABS, PLA and HIPS thermoplastics for structural applications. PSU Res. Rev. 2, 115–137

57. D. Therriault, et al. (2003). Chaotic mixing in three-dimensional microvascular networks fabricated by direct-wire assembly, Nat. Mater., 2, 265–271.

58. K. S. Toohey, et al. (2007). Self-healing materials with microvascular network. Nat. Mater., 6, 581–585.

59. C. J. Hansen, et al. (2009). Self-healing materials with interpenetrating microvascular networks. Adv. Mater., 21, 4143–4147.

60. A. R. Hamilton, et al. (2010). Self-healing of internal damage in synthetic vascular materials. Adv. Mater., 22, 5159–5163

61. Yu, et al. (2019). Additive manufacturing of self-healing elastomers. NPG Asia Materials. 11. 10.1038/s41427-019-0109-y.